JOURNAL OF CATALYSIS 136, 361–377 (1992)

Studies of Molybdena–Alumina Catalysts

XVIII. Lanthanum-Modified Supports

J.-W. CUI,*,[1] F. E. MASSOTH,*,[2] AND N-Y. TOPSØE†

*Department of Fuels Engineering, University of Utah, Salt Lake City, Utah 84112; and †Haldor Topsøe Research Laboratories, DK-2800 Lyngby, Denmark

Received November 21, 1991; revised March 23, 1992

A series of modified γ-alumina supports, to which 2–20% lanthanum was added, served as supports to prepare catalysts containing 6% Mo. The supports and catalysts were characterized, in the oxide and/or sulfide states, by XRD, ESCA, infrared spectroscopy, chemisorption of CO_2, and catalytic activity for thiophene hydrodesulfurization and hexene hydrogenation. The results showed evidence for strong interaction between the alumina and the lanthana, the latter forming a monomolecular overlayer on the alumina surface. At high La content, some La underwent sulfiding. The Mo interacted with the La–OH groups during calcination, forming essentially monolayer slabs of Mo-sulfide after sulfiding. Catalytic activities slightly decreased then increased with La loading, the latter being more pronounced for hydrogenation. Correlation of activities with NO adsorption from infrared measurements were interpretated in terms of a support effect of La on the Mo-sulfide active sites.

INTRODUCTION

Commercial hydrotreating catalysts commonly consist of CoMo or NiMo supported on a transition alumina, generally gamma- or eta-alumina. In a search for more active catalysts, a number of studies have been made using other oxides as supports, e.g., TiO_2 (*1–3*), ZrO_2 (*4, 5*), La_2O_3 (*5*), MgO (*2, 3*). The results have been mixed in that activities per Mo have been higher in some cases and lower in other cases compared to alumina. For example, at the same level of Mo, in one study (*1*) thiophene HDS activity decreased in the order $Al_2O_3 > SiO_2 > TiO_2$, while in another study (*3*) the order was the opposite. A problem with these supports is their inherent low surface area, so that only relatively low loadings of Mo could be achieved at monolayer capacity of the support.

In order to take advantage of the relatively high surface area of alumina, a number of basic studies have been carried out in which the alumina support was modified by addition of refractory oxides, e.g., MgO (*6–9*), TiO_2 (*6, 7, 10*). In these studies, the added oxide at low contents was generally well dispersed on the alumina, and the resultant Mo or Co(Ni)Mo catalysts exhibited either the same or somewhat lower hydrodesulfurization (HDS) activity compared to the alumina-based catalyst.

We are unaware of any similar studies done with lanthanum as an additive to alumina. The purpose of this research was to characterize La_2O_3 added to Al_2O_3 as supports for Mo catalysts.

EXPERIMENTAL

Supports and Catalysts

Supports were prepared by incipient wetness impregnation of a Ketjen 001 – 1.5 alumina, sieved to 20–40 mesh, with appropriate solution concentrations of lanthanum nitrate, followed by oven drying at 110°C

[1] 15 Dept., RIPP, P.O. Box 914, Beijing, 100083, P.R.C.

[2] To whom inquiries should be addressed.

0021-9517/92 $5.00

and calcination at 500°C for 16 hr. Supports are designated as Al–La (#), where the number in parenthesis is the approximate wt.% of La. Catalysts were prepared from these supports by impregnation with a solution of ammonium paramolybdate to give a final concentration after calcination of 6.0% Mo. Sulfiding of supports and catalysts was done in-situ with a flow of 10% H_2S/H_2 mixture at 400°C for 2 h, followed by an He purge for 2 h, all at atmospheric pressure. The He was purified by passing through a Hydrox trap.

Characterization

BET surface areas were measured with a Micromeritics analyzer. Sulfur analysis was accomplished by a standard combustion method. The OH content of the supports was determined by gravimetry, which consisted of measuring the weight of a sample at 500°C in a microbalance and then measuring the weight loss on heating to 1200°C in a muffle furnace, assuming no volatilization losses except water. X-ray analysis was performed on a Phillips diffractometer equipped with a graphite monochrometer and a copper X-ray tube, using powdered samples. The ESCA measurements were made on a Hewlett–Packard 5950B spectrometer using monochromatic Al*K* radiation (1486 eV). The details of the procedure are described elsewhere (*1*). Binding energies, corrected to 284.6 eV for C1*s*, gave the following in eV: La(3*d*5/2) = 835.6 ± 0.3 for Al–La and Mo/Al–La samples, Mo(3*d*5/2) = 233.7 for Mo/Al, and Mo(3*d*5/2) = 232.6 ± 0.3 for Mo/Al–La samples. Integrated peak areas were measured to obtain intensity ratios using standard photoelectron cross-sections.

Infrared measurements were made on both supports and calcined catalysts before and after sulfiding. The samples (40 mg) were ground and pressed into self-supporting wafers, which were sulfided *in situ* in the IR cell by passing a gas mixture consisting of 2% H_2S in H_2 at 450°C for 2 h, followed by an N_2 purge at 400°C for 14 h. The samples were then evacuated at room temperature to 10^{-6} Torr before adsorbing gases. All IR spectra were recorded using a Digilab FTS-80 Fourier Transform infrared spectrometer.

Chemisorption of CO_2 was measured on sulfided and He-purged samples by a pulse technique (*11*). This consisted in lowering the temperature of the sample after sulfiding *in situ* to 87°C in a stream of He, after which pulses of CO_2 were introduced every 3 min until no further adsorption was detected by a thermal conductivity cell.

Activity Measurements

Catalytic activities of *in-situ* sulfided catalysts were determined in a fixed-bed reactor at 350°C and atmospheric pressure. Thiophene was introduced by passing H_2 (60 cc/min) through bubblers held at 0°C, to which an auxiliary stream of 10% H_2S/H_2 (20 cc/min) was added. Conversions were obtained after 18 h on stream. The bubblers were subsequently switched to 1-hexene and conversions measured after 1–2 h on stream. Rate constants were calculated from conversions assuming first-order kinetics in the reactant.

RESULTS

A. Al–La Supports

1. Oxide Supports

Properties of the Al–La oxide supports are given in Table 1. Measured surface areas decreased with increase in La content. Calculated surface areas, *S*, assuming a monomolecular layer of La_2O_3 (*12*), are in good agreement with the experimental results. XRD analysis of the highest La-content sample showed only the presence of broad peaks attributable to the alumina. The results of ESCA analyses, shown in Fig. 1, demonstrate a high degree of dispersion of the La-oxide on the alumina up to the highest La loading. Studies on similar samples have shown that the La-oxide phase exists as monomolecular layers on the alumina surface (*13*), and a unit coverage of 19.3 Å^2

TABLE 1

Properties of Al–La Oxides Supports

	% La					
	0	2.0	5.3	11.3	20.0	Bulk La_2O_3
Surface area[a] (m^2/g)	220	217	216	192	167	23
S^b (m^2/g)	220	215	206	191	168	—
OH (mmol/g)	1.52	1.20	1.15	0.91	0.72	—
CO_2 adsorption (μmol/g)	82	—	—	—	269	60
La-oxide coverage (θ_L^*)[c]	0	0.077	0.214	0.49	0.99	—

[a] Experimental values.

[b] S is calculated surface area based on monolayer of La_2O_3; $S = 220(1 - 1.17 \times 10^{-3} \times [\text{wt. La}])$.

[c] Theoretical coverage of La-oxide monolayer on alumina surface, based on an area of 19.3 $Å^2$/La (*14*).

per La atom has been reported (*14*). Using this value, the theoretical fractional monolayer coverages of La-oxide, θ_L^*, of Table 1 were calculated. The La-oxide overlayer is envisioned as single-layer slabs of certain size on the alumina surface.

The OH content of the Al_2O_3 from the loss of water experiment gives an OH concentration of 4.1×10^{14} OH/cm^2, in good agreement with the literature for similarly calcined aluminas (*15, 16*). The OH content of the supports decreased with La loading (Table 1). Almost one-half of the original OH content was still left on the Al–La(20) sample. Figure 2 shows the infrared spectra of the hydroxyl stretching region of Al, Al–La(11), and Al–La(20) samples in their calcined state. The spectrum of Al_2O_3 shows the five distinctive OH bands characteristic of a partially dehydroxylated alumina surface (*17*). The intensity of these OH bands decreased significantly when La was added to the alumina, showing that the La has interacted extensively with the OH groups on the Al_2O_3 surface. At 20% La, some distinct OH bands can still be detected, but at lower intensity than that on the 11% La sample. The observation that the frequencies of the OH bands in the Al–La supports are slightly shifted from those of Al_2O_3 indicates that new OH species are formed, most likely La–OH groups.

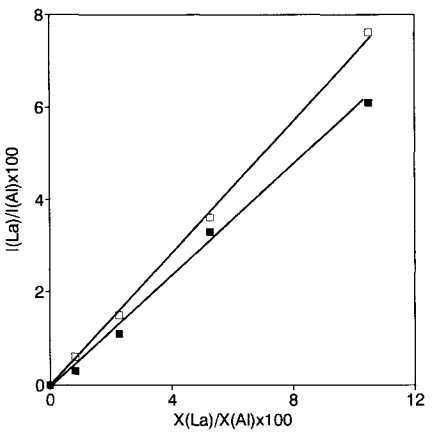

FIG. 1. ESCA La/Al intensity ratio vs La/Al composition mole ratio. Symbols: (□) Al–La supports; (■) Mo/Al–La catalysts.

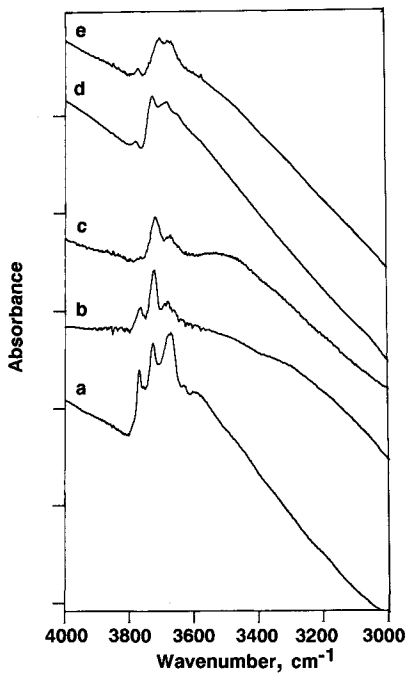

FIG. 2. IR spectra of the OH region of oxide samples: (a) Al, (b) Al–La(11), (c) Al–La(20), (d) Mo/Al, and (e) Mo/Al–La(11).

TABLE 2

Properties of Sulfided Al–La Supports[a]

	% La				
	0	2.0	5.3	11.3	20.0
Wt. sulfur (%)	<0.1	—	<0.1	0.7	1.8
m (μmol CO_2/g)	62	104	172	248	296
m/S (μmol CO_2/m^2)	0.28	0.48	0.83	1.30	1.76

[a] Values are per g oxide support.

2. *Sulfided Supports*

Properties of the sulfided supports are tabulated in Table 2. Sulfur analyses indicated that the Al and Al–La(5) supports did not undergo sulfiding, while the Al–La(11) and Al–La(20) supports showed partial sulfiding. The infrared spectrum of the OH region for the sulfided Al–La(11) support (not shown) was essentially the same as the oxide sample, indicating little effect of sulfiding on the OH concentration.

The infrared spectra for CO_2 adsorbed on these samples, given in Fig. 3, show significant differences between the samples. The sharp, CO_2-adsorption complex on the Al sample is considerably broadened, and the peaks are larger and shifted, clearly indicating that appreciably more CO_2 adsorbed on the La-oxide phase, in agreement with the adsorption data of Table 2. In the spectrum of Al–La(11), some band features similar to that of Al_2O_3 apparently are overlapped under the broad bands, indicating some remaining free Al_2O_3 surface.

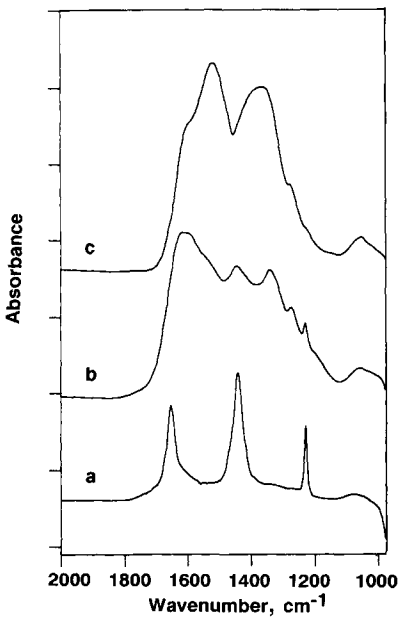

FIG. 3. IR spectra of CO_2 adsorbed on sulfided supports: (a) Al, (b) Al–La(11), and (c) Al–La(20).

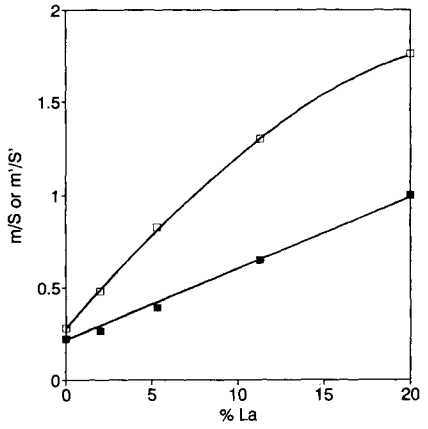

FIG. 4. Variation of CO_2 adsorption per surface area (m/S) with La content for: (□) sulfided supports (m/S); (■) sulfided catalysts (m'/S').

The CO_2 adsorption per surface area vs the La content of the oxide supports is shown in Fig. 4. An approximately linear relationship is obtained at low La loadings, which falls off for the two higher La-content supports. Adsorption of CO_2 has been employed to calculate surface coverage of La in similar samples (*13*), and this data will be used later to analyze possible surface models.

B. Mo/Al–La Catalysts

1. *Characterization*

a. Oxide catalysts. X-ray diffraction on the calcined (oxide) Mo/Al–La(20) catalyst failed to detect any phases of Mo or La. Figure 1 shows La/Al ESCA data on the oxide catalysts, which displays a good linear relationship with atomic ratio, indicating

TABLE 3

Properties of Sulfided Mo/Al–La Catalysts[a]

	% La				
	0	2.0	5.3	11.3	20.0
Mo/La (mol/mol)	—	4.8	1.81	0.84	0.48
S'[b] (m^2/g)	200	196	187	174	153
θ_T^M (Mo coverage)[c]	0.21	0.215	0.225	0.24	0.275
m' (μmol CO_2/g)	44.5	50.2	73.0	112.7	152.7
m'/S' (μmol CO_2/m^2)	0.22	0.26	0.39	0.65	1.00
$\Delta m'/S'$ (μmol CO_2/m^2)	0.06	0.22	0.44	0.65	0.76
k_T (cc/g-min)	13.2	11.0	6.5	7.0	8.9
C_T^d (%)	13	10	3	2	3
k_H (cc/g-min)	26.5	21.5	22.4	33.6	48.7
C_H^e (%)	8	4	0	0	0
HYD Sel.[f]	1.0	1.0	1.7	2.4	2.7

[a] All catalysts contain 6.0% Mo. Values are per g oxide catalyst.
[b] S' is calculated surface area based on monolayer of MoO_3; $S' = 0.91S$.
[c] Theoretical monolayer coverage of MoS_2.
[d] Ratio of products $<C_4$ to total hydrocarbon products.
[e] Ratio of products $<C_6$ to total hydrocarbon products.
[f] Ratio of k_H/k_T referred to Mo/Al catalyst.

that the addition of Mo to the Al–La supports has not changed the high dispersion of the La-oxide layer. The slightly lower slope of the line compared to the support probably signifies most of the Mo-oxide resides on top of La-oxide, else if most of the Mo was on the Al-oxide phase, the I_{La}/I_{Al} ratio would be expected to be slightly higher rather than lower. Infrared spectra for several of the oxide catalysts are shown in Fig. 2. These spectra show, as in the case of the Mo/Al catalyst, that incorporation of Mo-oxide on the Al–La supports greatly attenuates the OH bands, an indication of interaction between the Mo-oxide phase and the Al–La surface OH groups.

b. Sulfided catalysts. Sulfiding converts the Mo-oxide to an Mo-sulfide phase. Prior results with sulfided Mo/Al_2O_3 catalysts (*11*) have shown that at a content of 6% Mo, the Mo-sulfide phase is highly dispersed as monolayer slabs. Table 3 presents the characterization results for these catalysts. The surface areas were corrected for the amount of MoO_3 in the samples, assuming a monolayer of Mo-oxide. It is also assumed that the coverage of the La-oxide overlayer on the Al-phase remains the same as the sulfided supports.

Figure 5 displays infrared spectra of the OH region for the sulfided catalysts. There is little difference in the OH structure of the Mo/Al and the Mo/Al–La(2) catalysts. A decrease in the intensity of the OH bands is seen in the Mo/Al–La(5), and a more marked decrease is observed in the Mo/Al–La(11) and Mo/Al–La(20) catalysts. Also, there are small variations in the band frequencies; it is likely that the OH bands for the latter catalysts belong mainly to La–OH, which would indicate the presence of uncovered La surface in these catalysts.

Figure 6 presents infrared spectra for NO adsorbed on the sulfided Mo/Al–La samples. It is clearly seen that the NO absorbance decreased with increasing La loading. The relative intensity of the high and

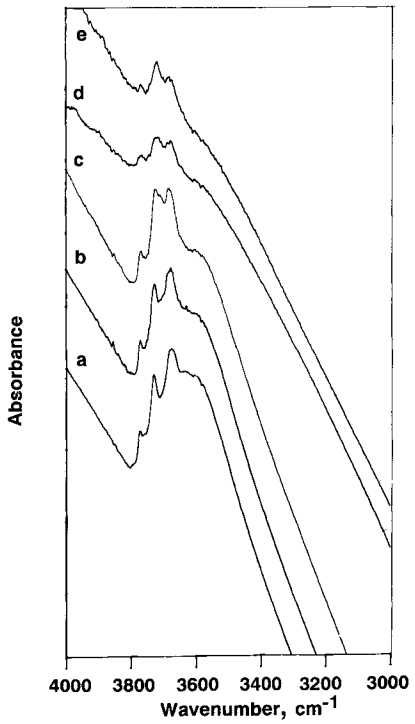

FIG. 5. IR spectra of OH region of sulfided catalysts: (a) Mo/Al, (b) Mo/Al–La(2), (c) Mo/Al–La(5), (d) Mo/Al–La(11), and (e) Mo/Al–La(20).

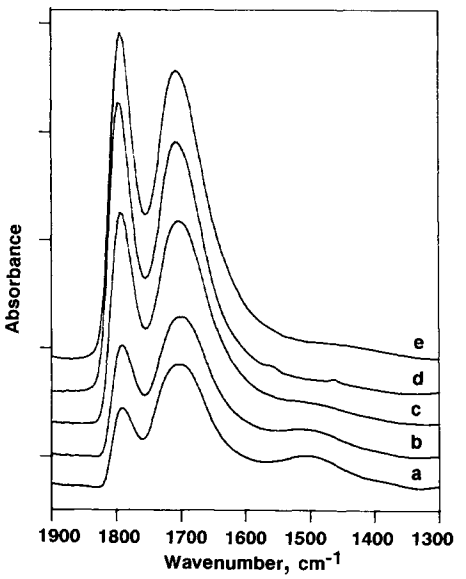

FIG. 6. IR spectra of NO adsorbed on sulfided catalysts: (a) Mo/Al–La(20), (b) Mo/Al–La(11), (c) Mo/Al–La(5), (d) Mo/Al–La(2), and (e) Mo/Al.

low frequency bands due to dinitrosyl species on the Mo is also seen to decrease progressively with increasing La. In addition, a new band at 1500 cm^{-1} appears, which becomes more pronounced at higher La content. These results indicate that the surface La-oxide phase also contains NO adsorption sites. The presence of this La–NO component signifies uncovered La surface, which increases with La concentration. This is in agreement with the limited (constant) amount of Mo present, which is insufficient to cover the La-oxide phase in the higher Mo/Al–La samples.

2. *Catalytic Activity*

The catalytic activities for HDS and hydrogenation (HYD) are given in Table 3 in terms of pseudo-first-order rate constants. The sulfided supports themselves showed very little HDS activity (k_T = 0.2–0.3 cc/g-min) and no HYD activity. The activities for the Mo-containing catalysts decreased at low La loading; whereas, at higher La content, HDS activity showed a slow recovery, while HYD activity markedly increased. The result is a dramatic increase in HYD selectivity with La loading. The presence of La also affected the hydrocracking activity of the catalyst (defined as the percentage ratio of cracked products to total products), giving substantial lowering in cracking activity with increase in La content.

3. *Correlation of Activities*

Previous studies (*18, 19*) on Mo/Al catalysts had shown, for the same support, good correlation between HDS activity and NO, that is, intrinsic activity (activity/NO) was constant, independent of Mo content. Since our catalysts all had the same amount of Mo, their activities might be expected to be the same. However, comparison of the IR(NO) absorbance data of Fig. 6 with the activity data of Table 3 shows an evident lack of a direct correlation between the two. In Fig. 7, relative intrinsic activities (ratio of activity/IR (Mo-NO) absorbance) are plotted against the La content. Two regimes of relative intrinsic activity are evident, viz. (i) low La loading—the relative intrinsic HDS activity slightly decreases, while the relative intrinsic HYD activity is little affected; and (ii) higher La loading—both increase with La content, the increase in HYD intrinsic activity being appreciably more pronounced.

MODELS

A. Al—La Supports

In this section we develop models of the oxide and sulfide supports based on the CO_2 data. Because data are lacking for the oxide supports, we first analyze the CO_2 data for the sulfided supports. Since the low La content supports did not undergo sulfiding, the CO_2 data for these supports are first analyzed. However, the CO_2 adsorption on the alumina did increase slightly upon sulfiding, due to a small amount of irreversibly retained H_2S (*20*).

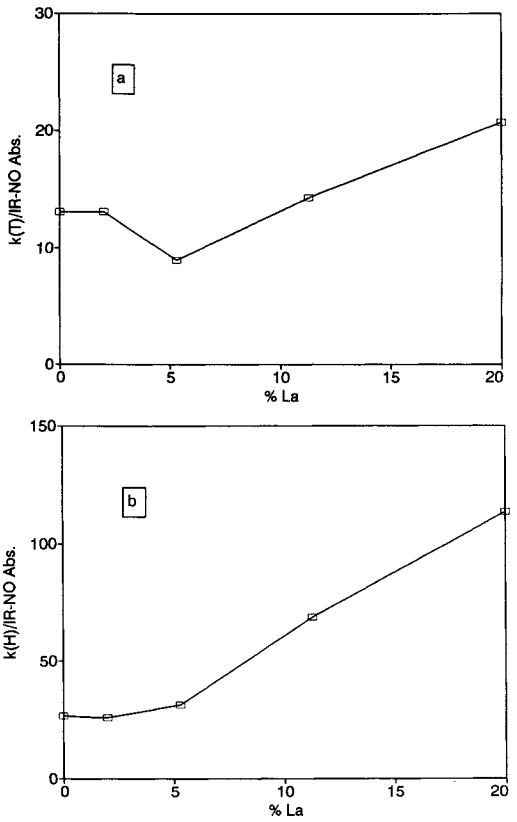

FIG. 7. Intrinsic activity (rate constant/IR-NO(Mo) absorbance) vs La content for (a) HDS; (b) HYD.

1. *Low La-Content Sulfide Supports*

For the Al–La(2) and Al–La(5) supports, the CO_2 uptake per surface area is given by

$$m/S = m_A/S + m_L/S$$
$$= (m_A/S_A)(S_A/S) + (m_L/S_L)(S_L/S), \quad (1)$$

where m_A and m_L are the contributions of CO_2 adsorption, while S, S_A, and S_L are the total surface area and the surface areas of the Al–O and La–O phases, respectively. The assumptions in Eq. (1) are (i) CO_2 adsorption on the exposed Al–O phase is the same for Al-La supports as for the alumina support, and, (ii) CO_2 adsorption per unit area on the La–O overlayer does not change with La content. Designating f_A for the amount of CO_2 adsorbed per unit area of the AlO phase (m_A/S_A), f_L for the amount adsorbed on the LaO phase per unit area (m_L/S_L), and as $S_L/S = \theta_L^*$ and $S_A/S = 1 - \theta_L^*$, Eq. (1) becomes

$$m/S = f_A(1 - \theta_L^*) + f_L\theta_L^*, \quad (2)$$

which rearranges to

$$f_L = [m/S - f_A(1 - \theta_L^*)]/\theta_L^*. \quad (3)$$

Substituting the appropriate values from Tables 1 and 2, where $f_A = m/S$ for sulfided Al_2O_3, leads to

$$f_L\,[\text{Al–La(2)}] = 2.88\ \mu\text{mol/m}^2$$
$$f_L\,[\text{Al–La(5)}] = 2.85\ \mu\text{mol/m}^2,$$

or an average adsorption per LaO layer of 2.86 μmol/m^2. A simplified model of this case is shown in Fig. 8b. Because these supports did not sulfide, the same model also applies to the oxide supports (Fig. 8a).

2. *20% La-Content Support*

For the high La-content support, it is evident from Fig. 4 that the CO_2 adsorption on the sulfided supports drops off at higher La loadings. This suggests that the monomolecular layer dispersion of the LaO phase is not maintained at high La levels. Accordingly, we first assume that a second layer of LaO(II) occurs on top of the first LaO(I) layer, as shown schematically in Fig. 8c, and designated as Case A. This model for the Al–La(20) oxide support seems reason-

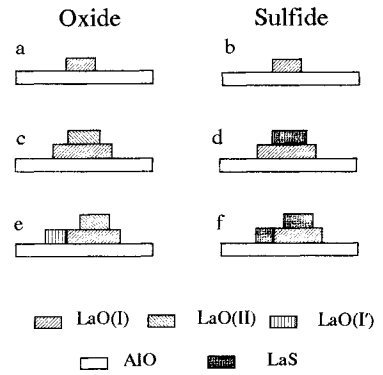

FIG. 8. Simple models for oxide and sulfide supports.

able as no evidence for large particles of bulk La_2O_3 were observed by XRD, and the ESCA results showed a high dispersion.

Next, we assume CO_2 adsorption on the second LaO(II) layer is similar to that on bulk La_2O_3, since this layer will partake of bulk La_2O_3–like character, being attached to LaO underneath rather than alumina. Thus, analysis for the Al–La(20) oxide support, according to the model of Fig. 8c gives

$$m/S = f_A[1 - \theta_L(I)] + f_L[\theta_L(I) - \theta_L(II)] + f_L'\theta_L(II), \quad (4)$$

where f_L' is the CO_2 adsorption on La_2O_3, given from Table 1, viz. 60/23 = 2.61 μmol/m^2. Now, θ_L^* gives the total coverage of both LaO phases, i.e., $\theta_L^* = \theta_L(I) + \theta_L(II)$. Substituting this into Eq. (4) and rearranging gives

$$\theta_L(II) = \frac{f_A + (f_L - f_A)\theta_L^* - m/S}{2f_L - f_A - f_L'}. \quad (5)$$

Substituting the appropriate values from Table 1 and the f values calculated above (now f_A = 0.37 for oxide alumina) gives

$$\theta_L(II) = 0.45, \quad \theta_L(I) = 0.54, \quad \theta_A = 0.46$$

for the Al–La(20) oxide support, according to model c in Fig. 8. Unfortunately, data are not available for the Al–La(11) oxide support, so we will use the sulfide support data to evaluate this support.

First we consider the case in which the LaO(II) phase completely sulfides to a LaS phase, i.e., Fig. 8d where LaO(II) becomes LaS. This assumes the same coverage of θ_S as for $\theta_L(II)$. This case is analogous to Eq. (4), where f_L' is replaced by f_S, adsorption of CO_2 per unit area of LaS. The latter is not known, but can be determined since the other values in Eq. (4) are known ($\theta_L(II) = \theta_S$ for this case). Thus,

$$f_S = \{m/S - f_A[1 - \theta_L(I)] - f_L[\theta_L(I) - \theta_L(II)]\}/\theta_L(II).$$

Substituting the appropriate values obtained above for the Al–La(20) oxide support (now f_A = 0.28 for sulfide alumina) yields f_S = 3.05 μmol/m^2. Using this value, θ_S can now be calculated for the Al–La(11) sulfide support via Eq. (5), with $\theta_L(II) = \theta_S$, which gives θ_S = 0.10.

TABLE 4

Predicted Surface Coverages for Sulfide Supports

% La	θ_A	θ_L	θ_S	θ'_S
0	1.00	0	0	na
2.0	0.91	0.08	0	na
5.3	0.79	0.21	0	na
11.3	0.61	0.39	0.10	na
		Case A		
20.0	0.46	0.54	0.45	na
		Case B		
20.0	0.45–0.46	0.44–0.54	0.44–0.45	0–0.11

Note. na—not applicable.

We now consider the more general case for the Al–La(20) support, in which part of the LaO(I) phase can also undergo sulfiding in addition to the LaO(II) phase. This is illustrated by Case B in Figs. 8e and 8f. The rationale for this case is that some of the La in the LaO(I) phase may not be strongly bonded to the AlO surface, and is susceptible to sulfiding. Case A considered above, where no LaO(I) sulfides, is then a limiting case of the more general Case B. The other limiting case is when no top layer LaO(II) exists, and part of the LaO(I) phase sulfides. It is shown in Appendix A, that the latter case does not agree with the CO_2 data.

For Case B, for the Al–La(20) oxide support (Fig. 8e), we have

$$m/S = f_A[1 - \theta_L(I) - \theta_L'(I')] + f_L[\theta_L(I) - \theta_L(II)] + f_L'[\theta_L'(I') + \theta_L(II)], \quad (6)$$

where the primes represent LaO, which resides on the alumina surface but is susceptible to sulfiding. Analysis of this case (Appendix B) does not permit determination of the individual θ's, but ranges can be determined. These are given in Table 4, Case B for the 20% La support (the same θ values apply to oxide and sulfide support, where $\theta_L(II) = \theta_S$ and $\theta_L'(I') = \theta_S'$). The results show

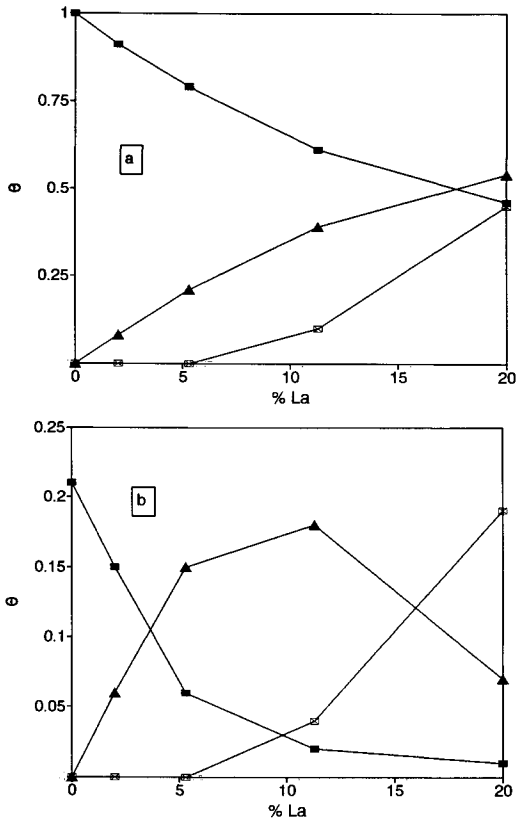

FIG. 9. Surface coverages for (a) sulfide supports and (b) sulfide catalysts. Symbols: (□) AlO; (▲) LaO; (⊠) LaS.

that $\theta'_L(I')$ must be less than 0.10, i.e., the majority of the sulfidable LaO is in the second layer. Applying the highest possible value of $\theta'_L(I')$ to analysis of the Al–La(20) sulfide support leads to $f_S = 2.92$, which is not too different from the value of 3.05 for Case A.

In summary, from the above analyses of the CO_2 adsorption data, all oxide supports can be described by the simple models of Case A shown in Fig. 8. A plot of coverages for the sulfided supports for Case A is given in Fig. 9a. It is seen that as the La content increases, the LaO-phase coverage (θ_L) increases, while the AlO phase (θ_A) decreases proportionally, as expected. The LaS-phase (θ_S) overlayer rapidly increases from 11 to 20% La, in agreement with the sulfur analyses of these supports (Table 2).

B. Mo/Al–La Catalysts

For the sulfide Mo/Al–La catalysts, MoS_2 could be present on each of the phases indicated in Fig. 8. This is shown schematically in Fig. 10, where the support coverages are those of Table 4.

Adsorption of CO_2 on the sulfided catalysts was always lower than on the sulfided supports (Fig. 4). Since CO_2 does not adsorb on the Mo-sulfide phase (*11*), the net loss indicates that the Mo-sulfide phase partially covers the various phases of the support. The net loss in CO_2 upon addition of Mo is given by

$$\Delta m'/S' = m/S - m'/S', \qquad (7)$$

where the primes refer to the catalyst. For the Mo/Al catalyst, this loss is simply given by

$$\Delta m'/S' = f_A \theta_A^M,$$

where θ_A^M is the coverage of MoS_2 on the alumina, which leads to $\theta_A^M = 0.06/0.28 = 0.21$. This value is in excellent agreement with the calculated value for monolayer slabs of MoS_2 of 0.20 (*11*). Therefore, the MoS_2 exists as monolayer slabs on the alumina surface.

For the low-La content sulfided catalysts,

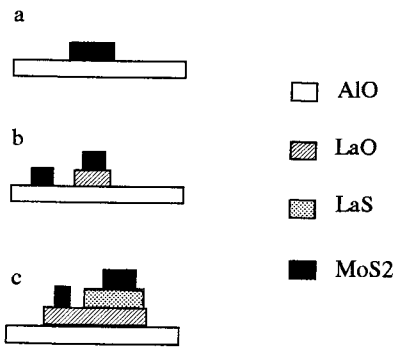

FIG. 10. Proposed models of sulfided catalysts. Blocks of the various phases represent their approximate respective overall surface coverage as given in Tables 4 and 5. The blocks are believed to occur as numerous small slabs rather than single blocks as shown.

the model of Figs. 10b or 10c leads to the following equation for the net loss in CO_2,

$$\Delta m'/S' = f_A\theta_A^M + f_L\theta_L^M, \quad (8)$$

where θ_L^M represents the coverage of MoS_2 on the LaO(I) phase. Assuming monolayer coverage of the MoS_2 on the both phases, then

$$\theta_T^M = \theta_A^M + \theta_L^M. \quad (9)$$

Since the same content of Mo was added to all the supports, while their surface areas decreased with La content, the actual coverage of Mo increased with La according to

$$\theta_T^M = 0.21 \times 200/S'.$$

Thus, Eq. (8) becomes

$$\theta_L^M = [\Delta m'/S' - f_A\theta_T^M]/(f_L - f_A). \quad (10)$$

Using the value of $f_L = 2.86$ obtained before, and the data of Table 3, the following coverages are obtained:

	Mo/Al–La(2)	Mo/Al–La(5)
θ_A^M	0.15	0.06
θ_L^M	0.06	0.15
$\theta_A^M/(1 - \theta_L^*)$	0.16	0.08
θ_L^M/θ_L^*	0.80	0.71

The lower set of values are the respective fractions of surface covered by the MoS_2 and show that the MoS_2 slabs occur preferentially on the LaO phase to the AlO phase.

Analysis of the CO_2 data for the high La-content catalysts is more involved. Now according to Figs. 10b or 10c, Eq. (8) becomes

$$\Delta m'/S' = f_A\theta_A^M + f_L\theta_L^M + f_S\theta_S^M, \quad (11)$$

where θ_S^M is the coverage of MoS_2 on the exposed LaS phase. Combination with

$$\theta_T^M = \theta_A^M + \theta_L^M + \theta_S^M \quad (12)$$

gives two equations with three unknown. However, ranges of the θ^M's consistent with the model can be obtained similar to that carried out above for the supports. Following a procedure similar to that described in Appendix B, i.e., by substituting one of the θ^M values to obtain an equation in the other two, the following permissible ranges for Case A were determined:

TABLE 5

Predicted MoS_2 Coverages for Sulfide Catalysts for Case A

% La	θ_T^M	θ_A^M	θ_L^M	θ_S^M
0	0.21	0.21	0	0
2.0	0.21	0.15	0.06	0
5.3	0.23	0.06	0.15	0
11.3	0.24	0.01 – 0.03 (0.02)	0.10 – 0.23 (0.18)	0 – 0.09 (0.04)
20.0	0.27	0.01 – 0.03 (0.01)	0 – 0.10 (0.07)	0.09 – 0.26 (0.19)

Note. Values in ( ) are "best" estimates (see text).

	Mo/Al–La(11)	Mo/Al–La(20)
θ_A^M	0.01–0.03	0.01–0.03
θ_L^M	0–0.26	0–0.25
θ_S^M	0–0.23	0–0.26

Since the MoS_2 coverage on the LaS phase cannot be greater than the LaS coverage, i.e., $\theta_S^M < \theta_S$, and likewise the MoS2 coverage on the exposed LaO phase cannot be greater than its coverage, i.e., $\theta_L^M < \theta_L - \theta_S^M$, the final allowable ranges become

	Mo/Al–La(11)	Mo/Al–La(20)
θ_A^M	0.01–0.03	0.01–0.03
θ_L^M	0.10–0.23	0–0.09
θ_S^M	0–0.10	0.16–0.26

A further refinement may be made by plotting θ_L^M vs $\theta_L - \theta_S$ for the 2 and 5% La catalysts (not given), which represents the MoS_2 coverage on the uncovered part of the LaO phase. The values of the 11 and 20% La catalysts can then be estimated from this plot, assuming the MoS_2 coverage is proportional to $\theta_L - \theta_S$. This gives estimated values of θ_L^M of 0.18 (11%) and 0.07 (20%), from which θ_S^M can be determined. These "best" values are given in Table 5. A plot of these

coverages is given in Fig. 9b. This plot shows that for the high La-content catalysts very little MoS_2 resides on the alumina surface, despite its appreciable remaining area. Thus, this analysis shows that the MoS_2 phase preferentially resides on the LaO phase, in agreement with the earlier conclusion that the Mo interacts with the LaO phase.

DISCUSSION

A. Al–La Supports

1. Oxide Supports

High-area transitional aluminas have been extensively studied (*15, 17, 21*). Of significance to the present study is the presence of hydroxyl groups at the surface of gamma-alumina calcined at 500°C. The IR spectrum of the alumina (Fig. 2) shows the presence of five OH bands, in agreement with the literature (*17, 21*). Hydroxyl groups may play an important role in stabilizing a high dispersion of a second oxide component on the alumina surface via interaction of OH groups of the two components, followed by dehydration during calcination with formation of oxygen linkages between the layers. For example, Mo can replace some of the OH groups on the alumina surface (*22, 23*). This results in essentially monolayer dispersion of the Mo, provided the loading does not exceed the monolayer capacity of the alumina. Monolayer dispersion has also been reported for titania supported on alumina (*24*).

For lanthanum oxide supported on alumina, essentially monomolecular layer dispersion has been reported up to a calcination temperature of about 800°C, without evidence of bulk La_2O_3 or mixed oxide compound formation (*13*). Our data, obtained at 500°C, are in general agreement, for example, the lack of a distinctive XRD pattern and the linear La/Al ESCA data with La loading. The residual OH content of the high La-content samples argues for the presence of some OH groups on the La-oxide layer. The infrared spectra of Fig. 2 clearly show a decrease in OH intensity when La is added, signifying interaction between the La-oxide and the alumina surface.

We envision reaction of La-hydroxylated species in solution to occur with Al–OH groups, as shown schematically in Scheme I. At low La content, the La-oxide interacts with some active OH sites on the Al_2O_3, which serve as nucleation centers for reaction. Subsequent additions of La result in growth of these initial La-oxide monomolecular patches, forming two-dimensional slabs on the alumina surface.

2. Sulfided Supports

At low to moderate La loadings, neither the Al–O nor the monolayer La–O phase undergoes sulfiding. For the Al–La(20) sample, the 1.8% S found clearly indicates that some of the La-oxide underwent sulfiding. This may be explained in terms of the reaction scheme given above, in which Al–O–La bonds are formed in the oxide state. When the Al–OH groups are used up, or are sufficiently weak, the excess La may deposit on top of the La-oxide overlayer as a second layer. This excess La-oxide apparently undergoes partial sulfiding.

Adsorption of CO_2 has been reported to occur on basic OH groups of alumina (*25*), and infrared studies have shown that CO_2 adsorbs on OH groups, forming bicarbonate or carbonate surface species on Al_2O_3 (*26*). O'Young *et al.* (*27*) found that the higher frequency peaks disappear after CO_2 adsorption and a new band around 3605 cm^{-1} appears. They assigned three peaks to bicarbonate species. Our IR data (Fig. 3) are consistent with their results. Bernal *et al.* (*28*) suggested the existence of hydroxycarbonate species on La_2O_3. The two relatively broad bands between 1360 and 1525 cm^{-1} in our spectrum are similar to their bands and reflect both the existence of bicarbonate species and the extent of heterogeniety of the surface (*29*), although the peak position is shifted because of

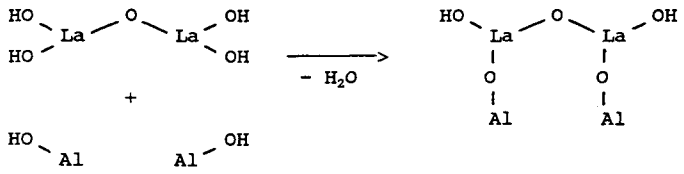

SCHEME I. Schematic representation of proposed interaction of La with alumina surface in oxide supports.

the interaction between La atoms and the Al_2O_3 surface.

B. Mo/Al–La CATALYSTS

1. Oxide State

The genesis of formation of the oxide and sulfide states of Mo on alumina has been the subject of several reviews (30–35), and the evidence will not be discussed here. The current consensus is that Mo-oxide species in solution react with some of the surface Al–OH groups, which upon calcination forms a surface "interaction species." Comparison of infrared spectra for Mo/Al vs Al_2O_3 in Fig. 2 clearly shows a loss in Al–OH groups upon addition of Mo.

We envision a similar process to take place with the La-oxide phase present in the Al–La supports, i.e., interaction of Mo-oxide species in solution with terminal La–OH groups present, to form upon calcination La–O–Mo linkages, with evolution of water. A possible schematic course of reaction is presented in Scheme II. Comparing the infrared spectra of Al–La(11) with Mo/Al–La(11) in Fig. 2, it is evident that Mo interacts with the Al–OH and/or La–OH groups.

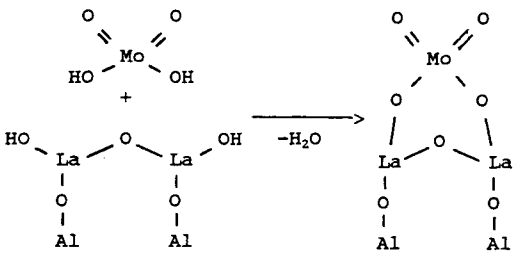

SCHEME II. Schematic representation of proposed interaction of Mo with La-oxide layer in oxide catalysts.

2. Sulfide State

Upon sulfidation, the Al–O–Mo linkages are mostly broken with formation of small, monolayer slabs of MoS_2 (*5, 36*), although a small fraction of the Al–O–Mo linkages may remain. Stuchly *et al.* (*37*) have recently reported that the number of OH groups on Mo/Al_2O_3 catalysts increases after sulfiding, showing regeneration of OH from rupture of Al–O–Mo bonds. Because of their small size and stoichiometry considerations, the MoS_2 slabs contain an appreciable fraction of sulfur anion vacancies (CUS sites) at their edges, and these are sites for NO adsorption and catalytic reaction.

Sulfidation of the Mo/Al–La oxide catalysts may also result in breaking the La–O–Mo linkages, as in the case with alumina, or may not, if they are sufficiently unreactive towards sulfiding. Comparison of the infrared spectra of Fig. 5 (sulfided) with Fig. 2 (oxide) for the Mo/Al–La(11) catalyst shows that OH groups are regenerated during sulfiding. It is expected that the Mo would be converted to the sulfide phase. One can see in the sulfided spectra of Fig. 5 that there is little difference in the OH structure of the Mo/Al and the Mo/Al–La(2) catalysts. A decrease in OH intensity is seen in the Mo/Al–La(5) catalyst, whereas a marked decrease is observed for the higher La-loaded catalysts. It is clear that both Mo and La interact with the Al–OH groups, and Mo must also interact with La–OH groups. It is likely that the OH bands observed for

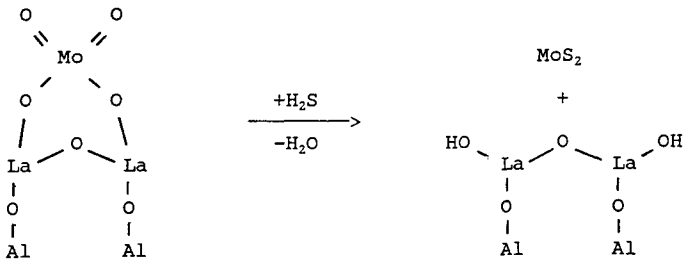

SCHEME III. Schematic representation of proposed sulfiding of Mo/La-oxide layer.

the higher La-loaded catalysts belong mainly to La–OH, which indicates the presence of uncovered La surface, as expected in view of the limited amount of Mo present. A possible course of sulfiding of Mo/Al–La catalysts is given in Scheme III. We envision partial breaking of the Mo–O–La bonds with reformation of some La–OH groups.

Adsorption of NO shows the characteristic infrared peaks of dinitrosyl species for the Mo/Al sample (Fig. 6), in agreement with prior studies (*38–40*). A new band at 1500 cm^{-1} appears, which becomes more pronounced at higher La loading. These results indicate that the surface La phase can form vacancies to accommodate NO. The presence of this La–NO component provides further evidence for uncovered La surface, which increases with increase in La content. Differences in the relative band intensities of the high and low frequency bands have been attributed to a difference in bond angle of the adsorbed dinitrosyl species (*41*). In our case, this may partly be due to adsorbed NO on the La phases, although this contribution appears to be small. The results shown in Fig. 6 clearly show that the Mo sites available for NO adsorption greatly decreased with increasing La content. The number of Mo adsorption sites already decreased at 2% La loading, which contributes only a very small coverage of the alumina surface. This decrease shows that some Mo must be on the LaO phase, in agreement with the models developed from the CO_2 adsorption data. Since considerable alumina surface is uncovered and Al–OH is left on the surface, this result suggests that Mo prefers the LaO phase.

The decrease in Mo–NO absorbance at higher La contents above 10% (Fig. 6) is not as drastic as that at the lower La levels, probably due to the fact that most of the Mo is now present on the La phase. Furthermore, it is seen that the uncovered La sites seem to reach a constant value at the high La concentrations, consistent with stacking of La layers on the alumina.

C. CATALYTIC ACTIVITY

1. HDS Activity

Since the Al–La supports showed essentially no conversion of thiophene, HDS activity is associated with the Mo-sulfide phase. A number of studies have found reasonable correlations between thiophene HDS activity and NO or O_2 adsorption for Mo/Al_2O_3 catalysts (*18, 42–45*). This means that the intrinsic activity (k_T/NO or k_T/O_2) should be invarient in Mo-sulfide slab size. Since the Mo loading in all our catalysts was the same, a constant intrinsic activity should be expected for all the Mo/Al–La samples, independent of MoS_2 slab size. Although the decrease in NO absorption is likely due to an increase in MoS_2 slab size, the intrinsic activity should not change, since the concentration of edge vacancies does not appreciably change with slab size (*46*). However, this was not the case, as seen in Fig. 7, where the HDS intrinsic activity dropped with La content and then gradually increased. We attribute these changes to a

support influence on the activity of the active sites on the Mo-sulfide slabs. The change in peak intensities with La content (Fig. 6) is an indication of differences in the character of the adsorption site, which presumably are reflected in differences in catalytic activity. Mauchasse *et al.* (*5*) reported that the support greatly influenced the activity of sulfided Mo in CO hydrogenation. A support influence has also been reported for sulfided Mo supported on TiO_2, where the HDS activity per NO adsorption was found to be higher than for Mo on Al_2O_3 (*47*).

The proposed models of Fig. 10 may provide an explanation for the changes in intrinsic activity obtained. From the activity data, relative to the alumina, the intrinsic activity of the MoS_2 on the La-oxide layer is lower, while that on the La-sulfide layer is higher. Thus, as the La content increases, increasing amounts of MoS_2 on the La-oxide layer results in lower overall activity, whereas at high La content, some MoS_2 resides on the second layer, increasing the net activity.

Lanthanum also has an effect on the selectivity of the thiophene reaction. The amount of cracking products deceased with increase in La content (Table 3). The decrease is in line with the HDS results, but more pronounced. This change in cracking pattern must also be associated with the La-oxide support. Since La_2O_3 is a basic oxide, the lowering in cracking activity may be associated with neutralization of the acidic sites on the alumina.

2. *HYD Activity*

Since hexene did not undergo hydrogenation over the Al–La supports, the HYD function is also exclusively associated with the Mo-sulfide phase. The pattern of HYD intrinsic activity with La content (Fig. 7) is similar to HDS intrinsic activity in that activity increases at high La loading. However, the effect is more pronounced. Furthermore, at low La levels, the HYD intrinsic activity is virtually unchanged. We may invoke the same explanation of support influence for HYD reactivity as for HDS activity presented above. However, the differences in intrinsic activity patterns would imply different sites, different combinations of sites, or different support electronic effects for the two reactions.

Desican and Amberg (*48*) had earlier proposed two different sites to be present on sulfided Mo/Al catalysts, a strongly acidic site responsible for hydrogenation of olefins and a weaker site predominately for HDS. Mann (*49*) has also proposed different sites for HDS and HYD, as have Stuchly and Beranek (*50*). Poisoning studies with sterically hindered and unhindered methyl-substituted pyridines by Miciukiewicz *et al.* (*51*) have shown that the sites for HDS of thiophene are geometrically restricted, while those for HYD of hexene are not. Further evidence for different sites has recently been reviewed by Massoth and Muralidhar (*31*). It is consequently reasonable to suppose that the support could have a different affect on the individual site activities.

3. *Support Effects*

In the above discussion we have invoked support effects to explain the trends in HDS and HYD activities. The global reaction rate consists of three factors: (i) the rate per active site; (ii) the number of active sites per edge area; and (iii) the edge area per total MoS_2 present. The initial decrease and subsequent increase in global rate with La content could be due to either of these factors.

We now attempt to identify which of these factors accounts for the different responses of the HDS and HYD activities with reference to the models of Fig. 10. For this purpose, we will compare the activities of the Mo/Al–La(2) and Mo/Al–La(20) catalysts with the MoS_2 phases present. Table 5 gives the MoS_2 coverages of each phase for these catalysts. The actual fraction of MoS_2 on each phase is given by $F_i = \theta_i^M/\theta_T^M$, since the same amount of MoS_2 was on each catalyst. This gives the following fractions:

	Mo/Al–La(2)	Mo/Al–La(20)
F_A	0.71	0.04
F_L	0.29	0.26
F_S	0	0.70

It is seen that F_L is about the same in both catalysts so that its contribution to catalytic activity should be about the same. Then, the major contribution to the activity of the 2% La catalyst can be considered as due to the MoS_2 on the AlO phase, while that of the 20% La catalyst is due to the MoS_2 on the LaS phase, both respective fractions being about the same. Now, the rate constant for HDS is lower for the 20% La catalyst than the 2% catalyst (8.9 vs 11.0), whereas the HYD constant is higher (48.7 vs 21.5). Thus, the HDS activity of the MoS_2 on the LaS phase is slightly lower than that on the AlO phase, but higher for HYD. Since the number of sites per edge area and the edge area per MoS_2 are the same for each reaction on the same catalyst, neither can account for the opposite effects on activities. Consequently, the differences in activities must be due to differences in the intrinsic rates per active site, i.e., an electronic influence of the support, which acts differently on the two reactions. Further, the NO adsorption on the MoS_2 for the 20% La catalyst is considerably lower than for the 2% catalyst (0.22 vs 0.72). This implies that the intrinsic activity per vacancy is higher for MoS_2 on the LaS phase than the AlO phase (since the amount on both is about the same). This may be due to less, but more active sites on the LaS phase.

CONCLUSIONS

La oxide (LaO) supported on alumina is present as a monomolecular layer strongly attached to the alumina surface. At high La loadings, a second LaO overlayer occurs on top of the first LaO layer. This second layer undergoes sulfiding. On addition of Mo, the Mo oxide reacts with both the Al oxide and the LaO phases, but preferentially the latter. Upon sulfidation, MoS_2 exists on both these phases, as well as on the sulfided second La layer.

The intrinsic activity of the MoS_2 phase was found to depend on the La loading in that a higher intrinsic activity was obtained at high La loading, which is attributed to an electronic influence of the underlying phase.

Differences in catalytic activity for the HDS of thiophene and the HYD of hexene are believed to be due to electronic support effects, which influence the two reactions differently.

APPENDIX A

Analysis of Oxide Support for No Second La Layer

According to this case for the Al–La(20) oxide support, all sulfidable LaO(II) resides on the alumina, but is sufficiently weakly attached as to partake of La_2O_3 character. Thus we assume $f'_L = 2.61$, as in Case A. Then

$$m/S = f_A[1 - \theta_L(I) - \theta_L(II)] + f_L\theta_L(I) + f'_L\theta_L(II).$$

Eliminating $\theta_L(I) = \theta^*_L - \theta_L(II)$ and solving for $\theta_L(II)$ yields

$$\theta_L(II) = \{f_L\theta^*_L + f_A(1 - \theta^*_L) - m/S\}/(f_L - f'_L).$$

Substituting the values $\theta^*_L = 0.99$, $m/S = 1.60$, $f_A = 0.37$, $f_L = 2.86$, and $f'_L = 2.61$ yields $\theta_L(II) = 4.9$. This result is clearly impossible, showing that this case does not agree with the analysis of the CO_2 adsorption data. Thus, according to this analysis, some LaO must occur as a second layer over the LaO(I) layer.

APPENDIX B

Analysis of Al–La(20) Oxide Support

For Case B, Fig. 8c, and the Al–La(20) oxide support, Eq. (6) applies. It is assumed that $\theta'_L(I')$, since it sulfides, is not strongly attached to the alumina, and therefore has

bulk La oxide character. Now

$$\theta_L^* = \theta_L(I) + \theta_L(II) + \theta'_L(I'). \quad (B1)$$

Because there are three unknown θ_L coverages and only two equations, each θ_L cannot be explicitly obtained. However, ranges of values can be obtained within the constraints of the model.

By elimination of $\theta_L(I)$ via Eq. (B1), and insertion into Eq. (6), solution for $\theta'_L(I')$ gives

$$\theta'_L(I') = \frac{f_A + (f_L - f_A)\,\theta_L^* - m/S - (2f_L - f'_L - f_A)\theta_L(II)}{f_L - f'_L}. \quad (B2)$$

In this case, $f_A = 0.37$ (oxide), $f_L = 2.86$ (same as Case A), and $f'_L = 2.61$ (same as Case A). Hence, Eq. (B2) becomes

$$\theta'_L(I') = [1.235 - 2.74\theta_L(II)]/0.25.$$

Thus, for $\theta'_L(I') > 0$, then $\theta_L(II)$ must be < 0.45.

A similar analysis eliminating $\theta_L(II)$ gives

$$\theta'_L(I') = [1.48 - 2.74\theta_L(I)]/2.49,$$

from which for $\theta'_L(I') > 0$, then $\theta_L(I) < 0.54$. In a like manner, elimination of $\theta'_L(I')$ gives

$$\theta_L(I) = [2.49\theta_L(II) - 0.99]/0.25, \quad (B3)$$

from which for $\theta_L(I) > 0$, $\theta_L(II) > 0.40$. Finally, since according to the model of Fig. 8e, $\theta_L(I) > \theta_L(II)$, then Eq. (B3) can be cast into the inequality

$$\theta_L(II) < 9.96\theta_L(II) - 3.96,$$

from which $\theta_L(II) > 0.44$. Thus, we obtain the allowable ranges of θ_L values given in Table 4, as the same values apply to the sulfide support, i.e., $\theta_L(I) \equiv \theta_L$, $\theta_L(II) \equiv \theta_S$, and $\theta'_L(I') \equiv \theta'_S$.

APPENDIX C: NOMENCLATURE

List of Symbols

f	CO_2 uptake (m/S or m'/S'), μmol/m^2
f'_L	CO_2 uptake on La_2O_3, μmol/m^2
m	CO_2 uptake, μmol/g support
m'	CO_2 uptake, μmol/g catalyst
$\Delta m'/S'$	net loss in CO_2 upon addition of Mo (Eq. (7)), μmol/g catalyst
S	calculated surface area, m^2/g support
S'	calculated surface area, m^2/g catalyst
θ	fractional surface coverage of phase
θ_L^*	theoretical fractional coverage of LaO phase for single layer
θ^M	fractional surface coverage of MoS_2 phase

Subscripts

A	AlO phase
L	LaO phase
S	LaS phase
T	total

ACKNOWLEDGMENT

Part of this research was supported by a DOE-Basic Sciences contract, which is gratefully acknowledged.

REFERENCES

1. Massoth, F. E., Muralidhar, G., and Shabtai, J., *J. Catal.* **85,** 53 (1984).
2. Nishjima, A., Shimada, H., Sato, T., Yoshimura, Y., and Hiraishi, J., *Polyhedron* **5,** 243 (1986).
3. Shimada, H., Sato, T., Yoshimura, Y., Hiraishi, J., and Nishijima, A., *J. Catal.* **110,** 275 (1988).
4. Reddy, B. M. P., Chary, K. V. R., Rama Rao, B., Subrahmanyam, V. S., and Nag, N. K., *Polyhedron* **5,** 191 (1986).
5. Mauchausse, C., Mozzanega, H., Turlier, P., and Dalmon, J-A., *in* "Proceedings, 9th International Congress on Catalysis, Calgary, 1988" (M. J. Phillips and M. Ternan, Eds.), Vol. 2, p. 775. Chem. Institute of Canada, Ottawa, 1988.
6. Muralidhar, G., Massoth, F. E., and Shabtai, J., *J. Catal.* **85,** 44 (1988).
7. Siani, A. R., Johnson, B. J., and Massoth, F. W., *Appl. Catal.* **40,** 157 (1988).

8. Jiratova, K., and Kraus, M., *Appl. Catal.* **27,** 21 (1986).
9. Martinez, N. P., and Mitchell, P. C. H., *in* "Proceedings, Climax Third International Conference on the Chemistry and Uses of Molybdenum (H. F. Barry and P. C. H. Mitchell, Eds.), p. 105. Climax Molybdenum Co., Ann Arbor, Michigan, 1979.
10. Yamagato, N., Pwada, Y., Okazaki, S., and Tanabe, K., *J. Catal.* **47,** 358 (1977).
11. Zmierczak, W., Qader, Q., and Massoth, F. E., *J. Catal.* **106,** 65 (1987).
12. Massoth, F. E., *J. Catal.* **50,** 190 (1977).
13. Bettman, M., Chase, R. E., Otto, K., and Weber, W. H., *J. Catal.* **117,** 447 (1989).
14. Xie, Y. C., Qian, M. X., and Tang, Y. Q., *Sti. Sin., Ser. B. (Engl. Ed.)* **27,** 549 (1984).
15. MacIver, D. S., Tobin, H. H., and Barth, R. T., *J. Catal.* **2,** 485 (1963).
16. Hall, W. K., Leftin, H. P., Cheselske, F. J., and O'Reilly, D. E., *J. Catal.* **2,** 506 (1963).
17. Peri, J. B., *J. Phys. Chem.* **69,** 211 (1965).
18. Miciukiewicz, J., Zmierczak, W., and Massoth, F. E., *Bull. Soc. Chim. Belg.* **96,** 915 (1987).
19. Massoth, F. E., Kim, C.-S., and Cui, J-W., *Appl. Catal.* **58,** 199 (1990).
20. Okamoto, Y., Oh-Hara, M., Maezawa, A., Imanaka, T., and Teranishi, S., *J. Phys. Chem.* **90,** 2396 (1986).
21. Knozinger, H., and Ratnasamy, P., *Catal. Rev.-Sci. Eng.* **71,** 31 (1978).
22. Segawa, K.-I., and Hall, W. K., *J. Catal.* **77,** 221 (1982).
23. Yasuak, O., and Toshinobe, I., *J. Phys. Chem.* **92,** 7102 (1988).
24. Stranik, M. A., Houalla, M., and Hercules, D. M., *J. Catal.* **106,** 362 (1987).
25. Boehm, H. P., *Discuss. Faraday Soc.* **52,** 264 (1972).
26. Parkyns, N., *J. Chem. Soc. A,* 410 (1969).
27. O'Young, C. L., Yang, C. H., DeCanio, S. J., Patel, M. S., and Storm, D. A., *J. Catal.* **113,** 307 (1988).
28. Bernal, S., Diaz, J. A., Garcia, R., and Rodriguez-Izquierdo, J. M., *J. Mater. Sci.* **20,** 537 (1985).
29. Rosynek, M. P., and Magnuson, D. T., *J. Catal.* **48,** 417 (1977).
30. Massoth, F. E., *Adv. Catal.* **27,** 265 (1978).
31. Massoth, F. E., and Muralidhar, G., *in* "Proceedings, Climax Fourth International Conference on the Chemistry and Uses of Molybdenum (H. F. Barry and P. C. H. Mitchell, Eds.), p. 343. Climax Molybdenum Co., Ann Arbor, Michigan, 1982.
32. Topsøe, H., Clausen, B. S., Topsoe, N-Y., and Pedersen, E., *Ind. Eng. Chem. Fundam.* **25,** 25 (1986).
33. Zdrazil, M., *Catal. Today* **3,** 269 (1988).
34. Delmon, B., *in* "Proceedings, Climax Third International Conference on the Chemistry and Uses of Molybdenum (H. F. Barry and P. C. H. Mitchell, Eds.), p. 73. Climax Molybdenum Co., Ann Arbor, Michigan, 1979.
35. Ratnasamy, P., and Sivashanker, S., *Catal. Rev.-Sci. Eng.* **22,** 401 (1980).
36. Clausen, B. S., Topsøe, H., Candia, R., Villardsen, J., Lengeler, B., Als-Nielsen, and Christensen, F., *J. Phys. Chem.* **85,** 3868 (1981).
37. Stuchly, V., Zahradnikova, H., and Beranek, L., *Appl. Catal.* **35,** 23 (1987).
38. Okamoto, Y., Katoh, Y., Mori, Y., Imanaka, T., and Teranishi, S., *J. Catal.* **70,** 445 (1981).
39. Topsøe, N-Y., *J. Catal.* **64,** 235 (1980).
40. Valyon, J., Schneider, R. L., and Hall, W. K., *J. Catal.* **85,** 277 (1984).
41. O'Young, C-L., *J. Phys. Chem.* **93,** 2016 (1989).
42. Reddy, B. M., and Subrahmanyam, V. S., *Appl. Catal.* **27,** 1 (1986).
43. Moon, S. J., and Ihm, S-K., *Appl. Catal.* **42,** 307 (1988).
44. Jung, H. J., Smitt, J. L., Ando, H., *in* "Proceedings, Climax Fourth International Conference on the Chemistry and Uses of Molybdenum (H. F. Barry and P. C. H. Mitchell, Eds.), p. 246. Climax Molybdenum Co., Ann Arbor, Michigan, 1982.
45. Bachlier, J., Duchet, J. C., and Cornet, D., *Bull. Soc. Chim. Belg.* **90,** 1301 (1981).
46. Miciukiewicz, J., and Massoth, F. E., *J. Catal.* **119,** 531 (1989).
47. Okamoto, Y., Maezawa, A., and Imaka, T., *J. Catal.* **120,** 29 (1989).
48. Desikan, P., and Amberg, C. H., *Can. J. Chem.* **42,** 843 (1964).
49. Mann, R. S., *Indian J. Technol.* **3,** 53 (1965).
50. Stuchly, V., and Beranek, L., *Appl. Catal.* **35,** 35 (1987).
51. Miciukiewicz, J., Zmierczak, W., and Massoth, F. E., *in* "Proceedings, 8th International Congress on Catalysis, Berlin, 1984," Vol. II, p. 671. Dechema, Frankfurt-am-Main, 1984.